



Photodegradation of dimethyldisulfide by heterogeneous catalysis using nanoCdS and nanoCdO embedded on the zeolite A synthesized from waste porcelain

Alireza Nezamzadeh-Ejhieh*, Zohreh Banan

Department of Chemistry, Shahreza Branch, Islamic Azad University, P.O. Box 311-86145, Shahreza, Isfahan, Iran
Tel. +98 321 3292515; Fax: +98 321 3291018; email: arnezamzadeh@iaush.ac.ir

Received 2 May 2012; Accepted 13 April 2013

ABSTRACT

Photodegradation of dimethyldisulfide (DMDS) was examined using nanoCdS and nanoCdO loaded on zeolite A as a heterogeneous catalyst under UV irradiation. Zeolite A was prepared from waste porcelain. Cadmium sulfide nanoparticles were prepared by a precipitation method using zeolite A as a template. Finally, CdO/A was prepared by wet impregnation of parent zeolite NaA with Cd(NO₃)₂ solution. Fourier transformation infrared, X-ray diffraction, and scanning electron microscopy methods were applied for the characterization of samples. UV–Vis spectrophotometric measurements were performed to determine the extent of decolorization and mineralization. Considering the influence of experimental parameters such as catalyst concentration, DMDS concentration, and pH of the test solutions, the contaminant photoelimination process was studied. The optimal operation parameters were found as follows: pH 1, 0.3 g L⁻¹ of catalyst loading, and 8 ppm of DMDS concentration. Based on the obtained results in the photodegradation process of DMDS, the most efficiency was detected in the presence of nanoCdS/A, while no remarkable activity was perceived when bulkCdS was used as the photocatalyst. CdO/A and nanoCdS particles also showed relatively good activities in the photodegradation extent of the contaminate. The degradation process obeyed first-order kinetics.

Keywords: Dimethyldisulfide; CdS nanoparticles; CdO; Photodecolorization; Zeolite A; Heterogeneous catalysis; Waste porcelain

1. Introduction

Dimethyldisulfide (DMDS) is one of the organosulfur compounds (OSCs) with high toxicity and characterized as a strong corrosive material. It is also one of the organic compound whose oxidation in the

atmosphere can produce sulfuric acid, which is the main component of acid rain [1]. It is released either by natural processes such as anaerobic biological activities or by anthropogenic sources, such as the Kraft paper pulping process which can lead to high local atmospheric concentrations of mercaptans [2]. It is also generated during poultry meat production [3] and is commonly found in various industrial processes, waste streams, and disposal facilities.

*Corresponding author.

To remove DMDS from waste streams several technologies have been reported, such as adsorption over activated carbon, thermal oxidation, biofiltration–bioscrubbling, and incineration; some of them are not that much suitable because of consuming high expense, high energy requirements, and high chemical consumption [3]. For example, because industrial wastewaters usually contain toxic and/or non-biodegradable organic substances, biological treatment is not efficient [2]. Photocatalytic oxidation is the most popular method to degrade different water pollutants such as OSCs [4–9]. In this method when a semiconductor is illuminated by a ray of light with a suitable wavelength, it generates electrons and holes which can further produce free radicals to decompose a large number of organic pollutants. Utilizing this method, OSCs and other pollutants are completely decomposed to minerals under mild conditions [10].

In most of the reports about photoremediation of pollutants, TiO_2 and ZnO have been used as photocatalyst [11–14]. In this research photodecolorization of DMDS by CdS nanoparticles incorporated with zeolite A was studied. To achieve this, cadmium sulfide nanoparticles were produced inside the channels and on the surface of zeolite A by precipitation after the ion exchange process. The obtained compound (nCdS/A) was used as a photocatalyst for decolorization of DMDS under UV irradiation. The photocatalyst exhibited a very good performance in destroying DMDS with consuming low expense and time. However, CdS anodic decomposition, the so-called photocorrosion, has limited its utility as a photocatalyst that has been explained in our previous work [15]. The use of a suitable sacrificial agent can overcome this disadvantage of the semiconductor. In general a mixture of Na_2S and Na_2SO_3 has been widely used as a sacrificial agent to prevent CdS photocorrosion.

2. Experimental

2.1. Materials

All chemicals were of analytical grade (Merck and Aldrich). The solutions were prepared with distilled water. Waste porcelain was prepared from Esfahan glass factory (Iran) and grounded by a mill. The grounded particles were washed with distilled water to use as a source of Si for preparing zeolite A. Table 1 shows the chemical composition of the used powdered waste porcelain. The pH of solutions was adjusted either by sodium hydroxide or hydrochloric acid solution.

Table 1
Chemical composition of the powdered waste porcelain (XRF)

| Compound | Percent |
|-------------------------|---------|
| LOI | 8.80 |
| SiO_2 | 64.41 |
| Al_2O_3 | 22.57 |
| K_2O | 1.47 |
| CaO | 0.972 |
| Na_2O | 0.783 |
| Fe_2O_3 | 0.438 |
| MgO | 0.245 |
| P_2O_5 | 0.076 |
| TiO_2 | 0.068 |
| SO_3 | 0.048 |
| SrO | 0.039 |
| MnO | 0.012 |
| ZnO | 0.008 |
| CuO | 0.007 |
| Total | 99.946 |

2.2. Zeolite preparation

Zeolite A was synthesized from waste porcelain at low temperature via a two-step alkali conversion [16]. In this method, during the first step, raw material (12.5 g) was added to a 4M NaOH solution (50 mL) and heated at 80°C for 12 h. At the end of the heating period, the reaction mixture was filtered; the Si and Al concentrations in the filtrate were analyzed by ICP. The concentration of Si and Al extracted from the waste were ca 20,000 and 10 ppm, respectively. The filtrate was then diluted 50% with distilled water. This diluted solution (2 mL) and aluminate solution (1 mL) were mixed to adjust the Si/Al molar ratio of 0.5. The mixed solution was heated at 80°C for 24 h. The resulting reaction mixture was filtered and the solid product was rinsed with distilled water, and dried in a drying oven at 60°C overnight.

2.3. Preparation of catalysts

2.3.1. Preparation of CdO embedded on zeolite A

Synthesis of CdO embedded on zeolite A was adapted from report [17]. It was prepared by wet impregnation of parent zeolite NaA with $\text{Cd}(\text{NO}_3)_2$ water solution (50.0 g/L). Impregnation was performed at 25°C for 2 h followed by drying at 100°C for 1 h and calcinations at 450°C for 6 h.

2.3.2. Preparation of CdS nanoparticles loaded on zeolite

The nCdS/A sample was prepared by a precipitation process using zeolite A as a matrix [18]. In a typical preparation procedure, 1 g Na-A was taken in a round bottom flask and 100 mL of a 1 M Cd(NO₃)₂ solution was added to it. The mixture was stirred for 24 h at room temperature. The zeolite was filtered and rinsed with distilled water until the filtrate was free from Cd²⁺ ions. The sample was dried and stirred with 100 mL of 1 M Na₂S solution for 12 h which resulted in the precipitation of the Cd²⁺ ions present in the zeolite matrix. The zeolite was then rinsed with distilled water until the filtrate was free from S²⁻ ions. A gray white color was observed following ion exchange with Cd²⁺ ions. It was then changed into a dark orange after the precipitation process, which can be considered as an initial evidence for the conversion of Cd²⁺ to CdS in the zeolite.

2.3.3. Preparation of nanoCdS

To prepare the nanoCdS sample, the obtained orange material was treated with a 48% HF solution, so that the zeolite matrix was removed. Then the insoluble nanoCdS particles were washed with hot water until the pH of filtrate became neutral [18].

2.3.4. Preparation of bulk CdS

The bulk CdS sample was synthesized by a conventional precipitation method. In this method, an equimolar amount of Na₂S solution was gradually added to a stirred solution of 1 M Cd(NO₃)₂ leading to the formation of CdS precipitates. The product was rinsed with distilled water several times, dried in an oven and then calcined at 400°C for 4 h [18].

2.4. Characterization

The chemical composition of the powdered waste porcelain was determined by X-ray fluorescence spectrometry (XRF) (Bruker, F4 Pioneer). The extracted Si and Al from waste porcelain were measured by ICP (GBC Integra XL). The X-ray diffraction (XRD) patterns of obtained zeolite A and nCdS/A was characterized by a Bruker diffractometer (D8 Advance) with Ni-filtered Cu K α radiation ($\lambda=1.5406$) over the 2θ range of 10–80°. Fourier transformation infrared (FT-IR) spectra of the samples on KBr pellets were recorded with a Nicolet single beam FT-IR (Impact 400D) spectrometer in the wave number range of

4,000–400 cm⁻¹ at room temperature. The surface morphology and surface texture properties of samples were obtained using a Philips XL30 scanning electron microscope (SEM) and a BET instrument (model Nova 1200), respectively. Atomic Absorption Spectrometer Perkin Elmer Analyst 300 (Air-C₂H₂, $\lambda=288.8$ nm) was the instrument to measure the amount of cadmium loaded on the zeolite.

2.5. Photodegradation experiments

In a typical photocatalytic experiment aqueous suspension (50 mL) of DMDS with certain concentration was fed through certain amount of the photocatalyst in a flat-surfaced glass reactor. A 75 W UV ($\lambda=200$ –430 nm) lamp was used and the distance between the lamp and glass-reactor was fixed at 30 cm. The reaction mixture was magnetically stirred during irradiation. To measure DMDS degradation efficiency, photometric analysis of samples before and after the irradiation can be used. The absorbance of the samples was measured using a UV-Vis spectrophotometer Carry 100 Scan. The concentration change was calculated from the linear calibration plot of DMDS at a wavelength of 251 nm. The degradation efficiency of the pollutant was determined by the following equation:

$$\text{Degradation \%} = \frac{C_0 - C}{C_0} \times 100$$

where C_0 and C are the initial and final (after irradiation) concentration of DMDS in selected time interval. During the degradation process, control experiments in dark condition were performed at the presence of catalysts and in accordance to each case to investigate the extent of surface adsorption.

3. Results and discussion

3.1. Characterization

3.1.1. XRD patterns

Fig. 1 shows the XRD pattern of zeolite A (ZA), nCdS/A and CdO/A samples. In the XRD pattern (curve a in Fig. 1) the characteristic lines at 2θ (7, 10, 12.5, 14.5, 16.1, 21.8, 23, 24, 26, 27.1, 30, 31, 32.5, and 34.2) values are observed that have a good agreement with the data of Na-A zeolite in the library of the instrument (JCPDS No. 38-0241) and in the literature [19]. This analysis showed that the product had a typical zeolite A structure as major component. The peaks correspond to the beta phase of the CdS particles

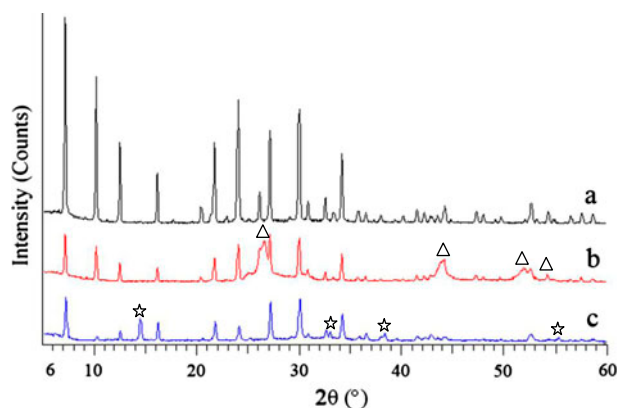


Fig. 1. XRD patterns of synthesized zeolite A (a), nanoCdS/zeolite A (b) and CdO/zeolite A (c); (Δ): CdS patterns and (*): CdO patterns.

(JCPDS No. 01-0647) located in the 2θ values of 26.5, 30.9, 44, 52, 54.5, 70.5, and 72.5. The most intense peaks are assigned as (Δ) in the pattern b in Fig. 1. The peaks which are not apparent in the ZA pattern, can illustrate the incorporation of CdS in the zeolite structure. According to JCPDS No. 05-0640, CdO should show some reflections in 2θ values of 14.5, 33, 38, 48.2, 55, 66, and 69. Some of these are present in the pattern c in Fig. 1, the most intense reflections corresponding to the XRD data of the CdO particles are assigned as (*).

Analysis of the β , excess of width line of the diffraction peak in radians and θ , the Bragg angle in degrees and using the Debye-Scherrer formula as [20]:

$$d = 0.9\lambda / \beta \cos \theta$$

where d is the average diameter of the crystal and λ the wavelength of X-ray, we determined the average size of ZA, NCdS-A and NCdO-A samples to be 2.8, 3.9, and 4.4 μm , respectively.

3.1.2. FT-IR spectroscopy

FT-IR spectra of the zeolite A, various types of CdS samples and CdO/A were recorded in the range of 4,000–400 cm^{-1} are shown in Fig. 2. Fig. 2(a) shows absorption peaks for bulk-CdS at 526.4, 615, 1,112, 1,629, and 3,506 cm^{-1} . The observed frequencies at 804, 1,086, 1,211, 1,635, 2,364, and 3,392 cm^{-1} in Fig. 2 (b), belong to the nano-CdS sample. According to the Fig. 2(c), the observed frequencies at 464, 562, 667, 1,016, 1,672, 3,033, and 3,479 cm^{-1} agree with the infrared spectral data, which have been reported for

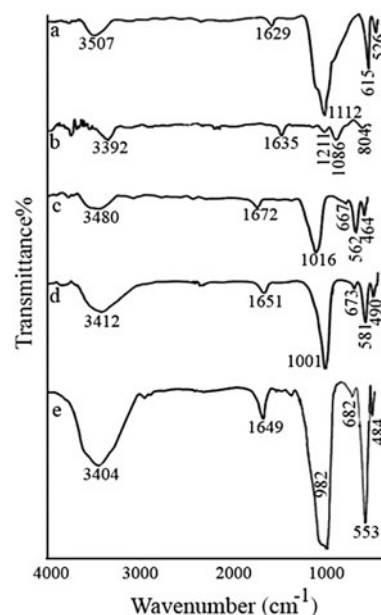


Fig. 2. FT-IR spectra of bulk CdS (a), nanoCdS (b), Zeolite A (c), nanoCdS/A zeolite (d), and CdO/A (e).

zeolite A [21]. The absorption frequencies of nano-CdS/A are shown in Fig. 2(d). Infrared spectroscopy can reflect the changes in the configuration of the frameworks of the zeolite host after the incorporation of the guests into the zeolite. The Changes of the characteristic peaks took place between the host zeolite A (the values in the parentheses) and the host-guest materials nanoCdS/A. For nanoCdS/A, the characteristic bands were 490 (464), 581 (562)(T–O bend), 673 (667) cm^{-1} (double rings), 1,001 (1,016) cm^{-1} (asymmetrical stretch), 653 (1,672), 3,412 (3,480) cm^{-1} which demonstrates a shift of some bands compared with the bands of the zeolite A host (Fig. 2(c) and (d)). These illustrate that nanoCdS particles have been embedded on zeolite A.

The absorption frequencies of CdO/A are shown in Fig. 2(e). The changes in the configuration of the frameworks of the zeolite host after the incorporation of the guests into the zeolite can be detected by infrared spectroscopy. Characteristic peak changes occurred between the host zeolite A (the values in the parentheses) and the host-guest materials CdO/A. For CdO/A, the characteristic bands were 484 (464), 553 (562) (T–O bend), 682 (667) cm^{-1} (double rings), 982 (1,016) cm^{-1} (asymmetrical stretch), 1,649 (1,672), 3,404 (3,480) cm^{-1} which demonstrates a shift of some bands compared with the bands of the zeolite A host (Fig. 2(c) and (e)). These illustrate that nanoCdS particles have been embedded on zeolite A.

3.1.3. SEM and BET analysis

The morphology of bulk CdS, nanoCdS particles, and CdS nano particles loaded on zeolite A was studied by SEM. The SEM photographs of the samples are present in Fig. 3. A regular growth pattern of fine particles of CdS in nano size range is clearly observed inside and on the surface of zeolite A as shown in Fig. 3(b)–(d). The surface of CdS nano particles is relatively rough in comparison to the bulk sample. The bulk sample with a large outgrowth of CdS particles in an irregular manner is illustrated in Fig. 3(a). Fig. 3 (e) and (f), shows nanoCdS particles and the zeolite matrix being removed by HF solution. The figures however do not show the complete removal of the matrix. The nano particles on the surface of zeolite A are in accordance with particle size distribution in the range of 48–68 nm.

BET surface area and micro pore volume were calculated by fitting the adsorption data in the corresponding theories and the obtained values are given in Table 2. According to results, the surface area of

the zeolite NaA increased by cadmium loading during the ion exchange process. This is due to the decrease in the number of extra-framework cations while replacing monovalent sodium cations with divalent cadmium cations. On replacing sodium cations with divalent cadmium cations, one Cd^{2+} replaces two Na^+ ions; therefore, half of the cation is present in the zeolite. The surface area and also the total pore volume of the CdO/A and CdS/A samples decreases due to blocking of some zeolite pores by the formation of CdO and CdS on the surface of zeolite. In general, the surface texture results are in coherence with the XRD results of particles sizes. The formation of CdO and CdS in zeolite channels and surface leads to an increase in the solid particle size and it is accompanied by a decrease in surface area and pore volume.

3.2. Catalytic activity of nCdS/zeolite A sample

A combination of nanoCdS particles and zeolite A provides a large specific area value to firstly adsorb

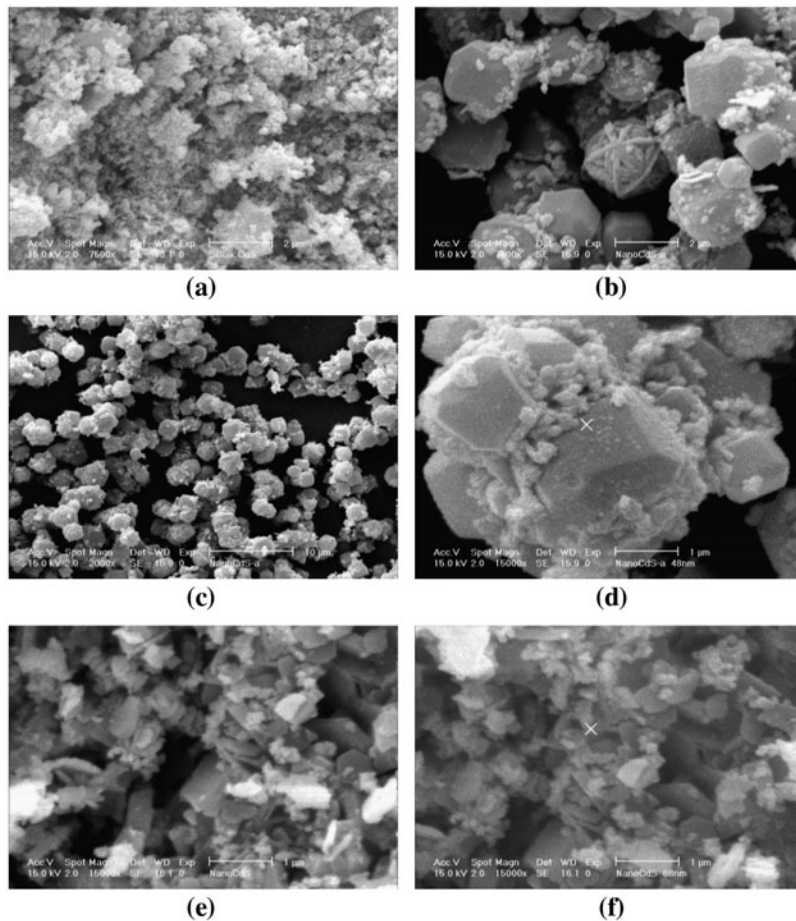


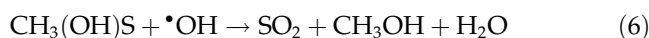
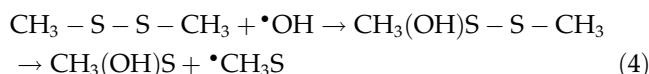
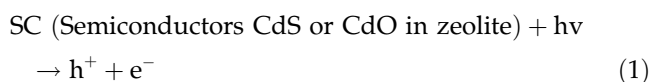
Fig. 3. SEM photographs of the bulk CdS (a), nCdS/A zeolite (b–d) and nanoCdS particles (e and f).

Table 2
Some surface characteristics of samples

| Sample | S_{BET} (m^2/g) | V_{p} (cm^3/g) | d_{p} (μm) |
|-----------|--|---|----------------------------------|
| NaA | 450 | 0.198 | 2.5 |
| CdA | 610 | 0.243 | 3.1 |
| Nano-CdSA | 415 | 0.157 | 3.5 |
| Nano-CdOA | 392 | 0.142 | 3.9 |

DMDS molecules and then oxidize them. Photodegradation could be performed directly by holes ($\text{DMDS} + \text{h}^+ \rightarrow \text{DMDS}^+$) or by the hydroxyl radical produced by reaction with hole and H_2O in situ generated. As the reaction environment in our experiments was aqueous the latter pathway could be the most important reaction happened during the photodegradation process.

Indeed, DMDS reacts with OH radicals to produce an intermediate ($\text{CH}_3(\text{OH})\text{SSCH}_3$) which is rapidly broken to form HCHO and SO_2 molecules by cleavage S–S bond [22]. Direct and indirect oxidation mechanisms both are explained in article [23]. FT-IR, ionic, and reverse phase chromatography have confirmed the formation of sulfate, methane sulfonate and the presence of C=O and methyl groups via photodegradation of DMDS [14,24]. Generation of the products mentioned above leads us to detect different types of reaction performing during the photodegradation of DMDS: (i) sulfur oxidation, (ii) carbon oxidation, and (iii) S–S bond cleavage [25]. Hence, we suggest the following mechanism for the degradation of DMDS.



The photocatalytic activity of nCdS/A in DMDS degradation was studied in detail. Also, the effects of

key operating parameters have been investigated. Fig. 4 demonstrates the UV–Vis spectra of degradation of a 8 ppm DMDS solution after UV irradiation in time period of 45 min in the presence of nCdS/A (0.3 g L^{-1}) as a photocatalyst. By the degradation of the pollutant, the decline of the sample's absorbance intensity at λ_{max} (251 nm) is indicated. To measure the degradation rate of DMDS, the decrease of the sample absorbance due to the decrease of DMDS concentration was recorded. Based on control experiment results, maximum value of DMDS surface adsorption stands at 18%, which was reflected on (was reduced from total degradation values) all degradation calculations.

3.2.1. Effect of photocatalyst dosage

The effect of catalyst dosage on the degradation extent of DMDS was investigated keeping all other experimental parameters constant. The results are shown in Fig. 5. Along increasing in dosage of the catalyst up to 0.3 g L^{-1} the rate of degrading also increased but beyond that, it decreased. The enhancement of catalyst loading from 0.1 to 3 g L^{-1} increased the degradation extent due to elevation of the catalyst surface area, which elevates absorption of photons and also increase the surface adsorption extent of pollutant. So the degradation extent of DMDS was enhanced. The diminish at high dosage beyond the optimum amount of 0.3 g L^{-1} is because of decreasing the light penetration and deactivation of activated molecules due to collision with the ground state molecules [26]. In addition, at higher catalyst dosage, suspension could not be remained homogenous easily because of particles condensation which decreases the number of active sites [27]. The decrease in the initial rate beyond the catalyst dosage of 0.3 g L^{-1} may also be attributed to the screening effect of excess catalyst particles in the solution which decreases the light penetration and hence reduces the photodegradation rate

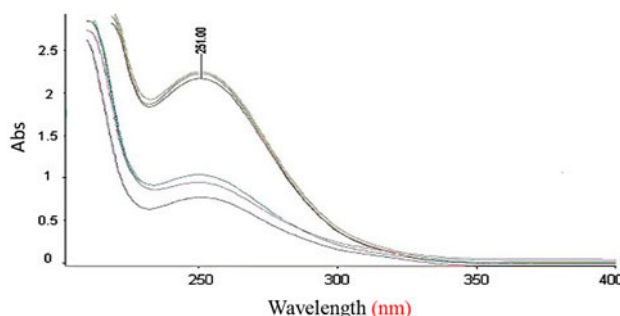


Fig. 4. Variation of the DMDS solution absorption spectral during the process in condition of 8 ppm of DMDS, $\text{pH}=8.2$, 0.3 g L^{-1} of nCdS/A and irradiation times of 8, 14, 21, 36, 60 and 90 min (from top to bottom).

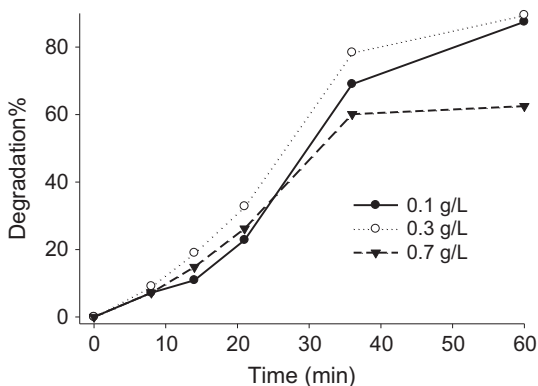


Fig. 5. Effect of nCdS/A dosage on the decolorization extent of DMDS, (initial concentration of DMDS=7 ppm and in its natural pH=8.2).

[28]. So, the overall number of the photons can be reached to catalyst particles and the production of OH radicals are decreased with the loading of the catalyst.

Based on our previous work, the kinetic of a photocatalytic reaction follows the first-order reaction [29]. To verify this, $\ln(C/C_0)$ was utilized as a function of the irradiation time. The results indicated that the first-order model gives a better fit. The constant rate values, k (min^{-1}), had to be determined from the straight-line portion of the first-order plots, as a function of the catalyst dosage and the obtained results are summarized in Table 3.

The amount of leached Cd^{2+} was also measured by atomic absorption spectroscopy, results the determination of cadmium ($\text{N}_2\text{O}-\text{C}_2\text{H}_2$ due to lower detection limit for Cd determination than $\text{Air}-\text{C}_2\text{H}_2$, $\lambda=288.8\text{ nm}$) and the obtained results showed no considerable Cd^{2+} in the solution. This is due to low solubility of CdS ($\text{pK}_{\text{sp}}=27.7$) in an aqueous solution.

Table 3
Reaction rate constants of DMDS degradation as a function of various experimental parameters

| Investigated parameter | Value | $k \times 10$ (min^{-1}) |
|-------------------------------------|-------|-------------------------------------|
| Catalyst mass (g L^{-1}) | 0.1 | 3.24 |
| | 0.3 | 4.23 |
| | 0.7 | 2.32 |
| C_{DMDS} (ppm) | 1 | 3.15 |
| | 2 | 3.32 |
| | 6 | 2.82 |
| | 8 | 5.85 |
| | 10 | 5.74 |
| | pH | 1 |
| 3 | | 3.74 |
| 7 | | 2.64 |
| 9 | | 1.22 |

This also shows photo corrosion of CdS which is very low due to small irradiation time.

3.2.2. Effect of DMDS concentration

Decolorization of DMDS catalyzed by nCdS/A under different DMDS initial concentrations was studied. DMDS act as a weak base and according to the used concentrations the pH of solutions were between 7.8 and 8.2. As it is shown in Fig. 6 the extent of degradation increases with increasing DMDS concentration up to 8 ppm, but above this concentration the efficiency decreases. The elevation of DMDS concentration causes decreasing catalytic efficiency and it could be explained with interface reaction processes. DMDS molecules are adsorbed onto zeolite A before they contact with nCdS active sites. Moreover, the hydroxyl radicals have very short lifetimes about a few nanoseconds and thus they should immediately react where they are formed. Hence, increasing the quantity of DMDS molecules per volume unit of the solution considerably enhances the probability of collision between DMDS molecules and oxidizing OH species, causing an increase in the degradation efficiency [20]. With increasing the initial concentration, a bigger amount of DMDS molecules could be adsorbed on the surface of the catalyst. This reduces generation of hydroxyl radicals because of the presence of fewer active sites for the adsorption of hydroxyl ions [20,30]. Also there is a competition between intermediate products of DMDS degradation and DMDS molecules for the limited adsorption sites and the result of the competition is blocking CdS active sites [30]. On the other hand, the decrease in efficiency in high concentration of DMDS could be attributed to insufficient number of OH radicals [31]. In addition, at higher concentrations of DMDS, some photons would be able

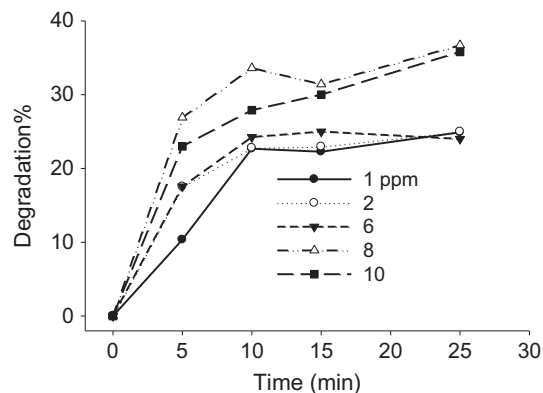


Fig. 6. Effect of initial concentration of the DMDS on the decolorization extent of the pollutant using 0.3 g L^{-1} of nCdS/A and in their natural pH=7.8–8.2.

to be absorbed by DMDS molecules before they could reach to catalyst surface. This in turn reduces absorption of photons by the catalyst and consequently generation of hydroxyl radicals and finally the degradation efficiency.

The constant rate value, k (min^{-1}), had to be determined from the straight-line portion of the first-order plots, the obtained results as a function of the DMDS concentration are summarized in Table 3.

3.2.3. Influence of initial solution pH

The pH of the solution affects on the photodegradation efficiency of the used catalyst due to the pH dependent of the different influencing properties such as semiconductor's surface charge state, flat band potential, and dissociation of compounds in the solution. In order to evaluate the influence of the initial solution pH, decomposition of DMDS in solutions with different pH from 1 to 9 was studied. As it is shown in Fig. 7, initial loss of DMDS was decreased by increasing in pH that may be explained with the different capacities of the surface of the catalyst in various pH values. The best degradation efficiency and also the rate constant values (as shown in Table 3) were observed at pH range of 1. In our idea the surface charge of the catalyst at various pHs plays an important role on the degradation extent of DMDS. In the strong acidic pHs, the charge of the surface of the catalyst is positive due to the high surface adsorption of protons by catalyst surface. The energy difference between 3p orbital of sulfur and 1s orbital of proton is high (with respect to 2p orbital of sulfur and 1s orbital of proton). This reduces the overlapping of free electron pairs of sulfur atoms in DMDS and the vacancy orbital of proton. On the other hand, in this condition the probability of protonation of free electron pairs of

sulfur atom is low. In this case, electro statistic force between the positive charge and free electron pairs of DMDS bring more DMDS molecules near the catalyst surface and hence the photodegradation efficiency increases. Hence, with increasing the pH, the surface charges of the catalyst being more negative. This increases the repulsion between the negative charges of the catalyst surface and free electron pairs of sulfur atoms. Hence, the degradation extent of DMDS decreases. At high concentration of OH^- (or higher basic pHs), reaction of $\bullet\text{OH}$ with OH^- yields H_2O_2 and $\text{HO}_2\bullet$ radicals. The reactivity of these radicals with pollutant is less than $\bullet\text{OH}$. In addition, due to the presence of high amounts of $\bullet\text{OH}$ radicals, the radical-radical reactions take place at higher pH values [32]. In our idea, with duration of time, some adsorbed DMDS molecules can be desorbed from the catalyst surface and cause to decrease in the removing efficiency of the process in higher irradiation times.

The rate constant value, k (min^{-1}), had to be determined from the straight-line portion of the first-order plots, the obtained results as a function of the solution pH are summarized in Table 3.

3.2.4. Effect of zeolite

To verify the influence of zeolite in DMDS degradation, the amount of nano CdS embedded onto the zeolite should be evaluated (via determination of Cd^{2+} by atomic absorption spectroscopy) which was found to be about 0.249 mmole CdS per gram of the catalyst. DMDS degradation efficiency by exposed nanoCdS particles (a 3 ppm nanoCdS suspension) was then studied under the same experimental conditions. The affinity of naked CdS nano particles for aggregation can explain the decrease in efficiency in the absence of the zeolite matrix. The role of the zeolite might be correlated with the adsorption process, in the sense of high surface area and the decrease of particle size [33]. In our idea, in the absence of zeolite, CdS particles tend to aggregate that causes a decrease in the active surface sites. But in the case of CdS incorporated zeolite, regarding to a small and definite pore size of zeolite, there are small particles of CdS in the zeolite that increase the available active sites of catalyst [34]. This in turn, causes an increase in the photodegradation efficiency. Catalytic efficiency of zeolite A during the degradation process was also studied in the above-mentioned conditions. Based on the achieved results no considerable degradation was exhibited in the absence of nano CdS particles. On the other hand, these results show that the responsible active centers for the degradation of DMDS are nano CdS particles loaded on the zeolite.

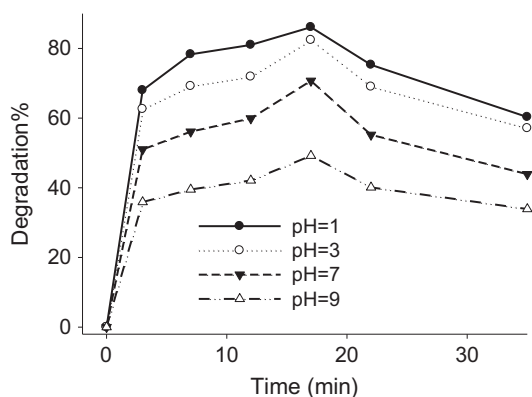


Fig. 7. Effect of solution pH on the decolorization efficiency of DMDS, (initial concentration of the pollutant = 8 ppm and 0.3 g L^{-1} nCdS/A).

3.2.5. A comparison between the photocatalytic activities of different catalysts

Fig. 8 shows DMDS decomposition efficiency under UV irradiation in the presence of different photocatalysts. As the graph shows no considerable degradation was observed when bulk CdS is used as the photocatalyst. It means that bulk CdS has not a good photocatalytic activity for DMDS degradation. It is also seen that CdS nano particles decompose DMDS in a higher rate in comparison with that of the bulk CdS sample. On the other hand, due to aggregation of bulk CdS particles the ratio of catalyst surface to volume will reduce. Decrease in the effective surface area of bulk CdS decrease the available active CdS sites to expose with photons and also surface adsorption of the pollutant molecules. These in turn decreases the degradation extent of DMDS [30,35]. Indeed the number of electron/hole pairs on the surface of a semiconductor verifies photocatalyst reactivity. For semiconductors with large particles, the distance the electron/hole pairs have to move from crystal edge to the surface of photocatalyst is rather long. Therefore, the possibility of electrons/holes recombination during immigration time is increased. But in the case of nano particles, the travel length is short and electrons/holes can participate in the reaction process before recombination [35–38]. Therefore nano-scale semiconductors are superior to their bulk counterparts due to the changes in band-gap, morphology, surface area, and generating surface defects.

However as the graph shows, naked nano CdS particles demonstrate lower reactivity in comparison with nano CdS/A in DMDS degradation process. The high accessibility of CdS when it is gathered inside

the zeolite channels, the presence of zeolite as a secure host to support the loaded CdS particles from photo-corrosion, and the polarization power of the zeolite channels could prevent charge recombination between electrons and holes that causes increasing CdS activity. Therefore, zeolites with cages and channels to prepare controlled particle size of semiconductors, higher surface area, unique nano-scaled pores structure, ion exchange properties, thermal stability, hydrophobic, and hydrophilic properties and eco-friendly nature can be used as a confident system to cooperate with semiconductors for creating an efficient photodegradation process [39]. It is also seen in the graph that using CdO/A as the photocatalyst leads the degradation process to continue with a higher rate in comparison with bulk CdS, and lower rate in comparison with the other mentioned CdS samples. This issue can be explained by the fact that particle size, band-gap energy, the crystal structure, morphology, phase composition, size, and shape of a semiconductor determine its photoreactivity [40]. It can be also clarified with the lack of zeolite in the bulk CdS system during photocatalysis process. The photocatalytic efficiency also depends on the adsorption dynamics of substrate and intermediates, the electronic interaction between semiconductor and adsorbates, and the band structure [41]. To close the above research, the photodecomposition efficiency is found to decrease in the order:

nanoCdS/A > nanoCdS > CdO/A > bulk CdS.

The results of the present work agree with those of our previous work [9].

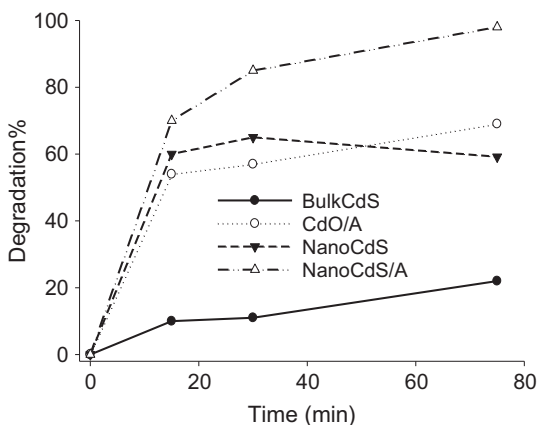


Fig. 8. Effect of zeolite in the decolorization process of DMDS, (initial concentration of the pollutant = 8 ppm, DMDS natural pH = 8.2 and 0.3 g L^{-1} nCdS/A).

4. Conclusions

Nano CdS particles loaded on zeolite A can be utilized as the main active centers for decomposition of DMDS aqueous solution under UV irradiation in a photodegradation process. The photocatalyst shows more activity compare to CdO/A, the naked and bulk CdS particles. In the presence of nano photocatalyst the degradation efficiency is increased due to increasing in active surface of photocatalyst and also accelerating in traveling rate of electrons/holes to the surface of the catalyst. The Zeolitic bed is as a support in this study which helps photodegradation process becomes more efficient. The use of a combination of nano CdS as a photocatalyst and zeolite A as a support render the reaction interesting from both economical and environmental points of view and therefore, this system facilitates its industrial applications.

References

- [1] L.R. Bentley, T.G. Chasteen, Environmental VOSCs-formation and degradation of dimethyl sulfide, methanethiol and related materials, *Chemosphere* 55 (2004) 291–317.
- [2] S. Sivelä, Dimethyl Sulphide as a growth substrate for an obligately chemolithotrophic thiobacillus, *Societas Scientiarum Fennica, Helsinki*, 1 (1980) 1–69.
- [3] R.L. Krügera, R.M. Dallago, M.D. Luccio, Degradation of dimethyl disulfide using homogeneous Fenton's reaction, *J. Hazard. Mater.* 169 (2009) 443–447.
- [4] P.R. Gogate, A.B. Pandit, A review of imperative technologies for wastewater treatment I: Oxidation technologies at ambient conditions, *Adv. Environ. Res.* 8 (2004) 501–551.
- [5] H.R. Pouretedal, H. Motamedi, A. Amiri, Aromatic compounds photodegradation catalyzed by ZnS and CdS nanoparticles, *Desalin. Water Treat.* 44 (2012) 92–99.
- [6] A. Nezamzadeh-Ejhih, S. Moeinirad, Heterogeneous photocatalytic degradation of furfural using NiS-clinoptilolite zeolite, *Desalination* 273 (2011) 248–257.
- [7] A. Nezamzadeh-Ejhih, M. Khorsandi, A comparison between the heterogeneous photodecolorization of an azo dye using Ni/P zeolite and NiS/P zeolite catalysts, *Iran. J. Catal.* 1(2) (2011) 99–104.
- [8] H. Faghiliani, A. Bahrnifard, Application of TiO₂-zeolite as photocatalyst for photodegradation of some organic pollutants, *Iran. J. Catal.* 1 (2011) 45–50.
- [9] A. Nezamzadeh-Ejhih, Z. Banan, A comparison between the efficiency of CdS nanoparticles/zeolite A and CdO/zeolite A as catalysts in photodecolorization of crystal violet, *Desalination* 279 (2011) 146–151.
- [10] A. Nezamzadeh-Ejhih, M. Amiri, CuO supported clinoptilolite towards solar photocatalytic degradation of p-aminophenol, *Powder Technol.* 235 (2013) 279–288.
- [11] P. Bansal, N. Bhullar, D. Sud, Studies on photodegradation of malachite green using TiO₂/ZnO photocatalyst, *Desalin. Water Treat.* 12 (2009) 108–113.
- [12] N. Gonzalez-Garcia, J.A. Ayllon, X. Domenech, J. Peral, TiO₂ deactivation during the gas-phase photocatalytic oxidation of dimethyl sulfide, *Appl. Catal. B: Environ.* 52 (2004) 69–77.
- [13] A.V. Vorontsov, E.N. Savinov, C. Lion, P.G. Smirniotis, TiO₂ reactivation in photocatalytic destruction of gaseous diethyl sulfide in a coil reactor, *Appl. Catal. B: Environ.* 44 (2003) 25–40.
- [14] C. Guillard, D. Baldassare, C. Duchamp, M.N. Ghazzal, S. Daniele, Photocatalytic degradation and mineralization of a malodorous compound (dimethyl disulfide) using a continuous flow reactor, *Catal. Today* 122 (2007) 160–167.
- [15] A. Nezamzadeh-Ejhih, Z. Banan, Sunlight assisted photodecolorization of crystal violet catalyzed by CdS nanoparticles embedded on zeolite A, *Desalination* 284 (2012) 157–166.
- [16] T. Wajima, Y. Ikegami, Synthesis of zeolitic materials from waste porcelain at low temperature via a two-step alkali conversion, *Ceram. Int.* 33 (2007) 1269–1274.
- [17] M. Brazlauskas, S. Kitrys, Synthesis and properties of CuO/zeolite sandwich type adsorbent-catalysts, *Chin. J. Catal.* 29 (2008) 25–30.
- [18] M. Sathish, B. Viswanathan, R.P. Viswanath, Alternate synthetic strategy for the preparation of CdS nano particles and its exploitation for water splitting, *Int. J. Hydrogen Energy* 31 (2006) 891–898.
- [19] H. Robson, Verified synthesis of zeolitic materials, *Micropor. Mesopour. Mater.* 22 (1998) 551–666.
- [20] A. Nezamzadeh-Ejhih, K. Shirvani, CdS Loaded an Iranian clinoptilolite as a heterogeneous catalyst in photodegradation of p-aminophenol, *J. Chem.* 2013 (2013) 11, Article ID 541736.
- [21] E.M. Flanigen, H.A. Szymanski, *Molecular Sieve Zeolites Advances in Chemistry Series*, vol. 101, American Chemical Society, Washington, DC, 1971, pp. 201–208.
- [22] S. Hatakeyama, H. Akimoto, *J. Phys. Chem.* 87 (1983) 2387–2395.
- [23] K. Demeestere, J. Dewulf, B.D. Witte, H.V. Langenhove, Titanium dioxide mediated heterogeneous photocatalytic degradation of gaseous dimethyl sulfide: Parameter study and reaction pathways, *Appl. Catal. B: Environ.* 60 (2005) 93–106.
- [24] R.M. Silverstein, G. Clayton Bassler, T.C. Morill (Eds.), *Spectrometric Identification of Organic Compounds*, 5th ed., John Wiley and Sons, New York, NY, 1991.
- [25] J.R. Agger, N. Pervaiz, A.K. Cheetham, M.W. Anderson, Crystallization in zeolite A studied by atomic force microscopy, *J. Am. Chem. Soc.* 120 (1998) 10754–10759.
- [26] A. Nezamzadeh-Ejhih, Z. Salimi, Heterogeneous photodegradation catalysis of o-phenylenediamine using CuO/X zeolite, *Appl. Catal. A: Gen.* 390 (2010) 110–118.
- [27] H.R. Pouretedal, S. Sabzevari, Photodegradation study of congo red, methyl orange, methyl red and methylene blue under simulated solar irradiation catalyzed by ZnS/CdS nanocomposite, *Desalin. Water Treat.* 28 (2011) 247–254.
- [28] A. Nezamzadeh-Ejhih, Z. Salimi, Solar photocatalytic degradation of o-phenylenediamine by heterogeneous CuO/X zeolite catalyst, *Desalination* 280 (2011) 281–287.
- [29] A. Nezamzadeh-Ejhih, M. Khorsandi, Heterogeneous photodecolorization of Eriochrome black T using Ni/P zeolite catalyst, *Desalination* 262 (2010) 79–85.
- [30] A. Nezamzadeh-Ejhih, M. Khorsandi, Photodecolorization of Eriochrome black T using NiS-P zeolite as a heterogeneous catalyst, *J. Hazard. Mater.* 176 (2010) 629–637.
- [31] M. Mahalakshmi, S. Vishnu Priya, B. Arabindoo, M. Palanichamy, V. Murugesan, Photocatalytic degradation of aqueous propoxur solution using TiO₂ and H β zeolite-supported TiO₂, *J. Hazard. Mater.* 161 (2009) 336–343.
- [32] A. Nezamzadeh-Ejhih, E. Shahriari, Heterogeneous photodecolorization of methyl green catalyzed by Fe(II)-o-phenanthroline/zeolite Y nanocluster, *Int. J. Photoenergy* 2011 (2011) 10, Article ID 518153.
- [33] M.B. Kasiri, H. Aleboyeh, A. Aleboyeh, Degradation of acid blue 74 using Fe-ZSM5 zeolite as a heterogeneous photocatalyst, *Appl. Catal. B* 84 (2008) 9–15.
- [34] M. Alvaro, E. Carbonell, M. Espla, H. Garcíá, Iron phthalocyanine supported on silica or encapsulated inside zeolite Y as solid photocatalysts for the degradation of phenols and sulfur heterocycles, *Appl. Catal. B: Environ.* 57 (2005) 37–42.
- [35] V. Ramamurthy, K. Schanze, *Molecular and Supramolecular Photochemistry, Organic Photochemistry*, vol. 1, Marcel Dekker, New York, NY, 1997, (Chapter 7), pp. 245–294.
- [36] M.A. Barakat, H. Schaeffer, G. Hayes, S. Ismat-shah, Photocatalytic degradation of 2-chlorophenol by Co-doped TiO₂ nanoparticles, *Appl. Catal. B: Environ.* 57 (2004) 23–30.
- [37] B. Pal, T. Torimoto, K. Iwasaki, T. Shibayama, H. Takahashi, Size and structure-dependent photocatalytic activity of jinglebell-shaped silica-coated cadmium sulfide nanoparticles for methanol dehydrogenation, *J. Phys. Chem. B* 108 (2004) 18670–18674.
- [38] M. Warrior, M.K.F. Lo, H. Monbouguet, M.A. Garcia-Garibay, Photocatalytic reduction of aromatic azides to amines using CdS and CdSe nanoparticles, *Photochem. Photobiol. Sci.* 3 (2004) 859–863.
- [39] A. Nezamzadeh-Ejhih, S. Hushmandrad, Solar photodecolorization of methylene blue by CuO/X zeolite as a heterogeneous catalyst, *Appl. Catal. A: Gen.* 388 (2010) 149–159.
- [40] A. Testino, I.R. Bellobono, V. Ba, C. Canevali, M. D'Arienza, S. Pollizi, R. Scotti, F. Morazzoni, Optimizing the photocatalytic properties of hydrothermal TiO₂ by the control of phase composition and particle morphology, a systematic approach, *J. Am. Chem. Soc.* 129 (2007) 3564–3575.
- [41] T. Tachikawa, M. Fujitsuka, T. Majima, Mechanistic insight into the TiO₂ photocatalytic reactions: Design of new photocatalysts, *J. Phys. Chem. C* 111 (2007) 5259–5275.